Non-parametric statistical techniques for the truncated data sample: Lynden-Bell's C^- − method and Efron-Petrosian approach

Anastasia Tsvetkova
on behalf of the Konus-*Wind* team
Ioffe Institute

Contents

- Parametric vs non-parametric techniques
- Konus-*Wind* experiment
- The burst sample
- The sample analysis
- Selection effects
- GRB detection horizon
- Non-parametric statistical techniques for a truncated data sample
- Luminosity (energy release) evolution
- GRB luminosity and energy release functions
- GRB formation rate
- Summary

Parametric vs non-parametric techniques

	Parametric	Non-parametric ("distribution-free")
Assumed distribution	Predictable (and often Normal)	Any
Assumed variance	Homogeneous	Any
Typical data	Ratio or Interval	Ordinal or Nominal
Data set relationships	Independent	Any
Usual central measure	Mean	Median
Benefits	Can draw more conclusions	Simplicity; Less affected by outliers

Parametric vs non-parametric techniques

Tests	Parametric	Non-parametric
Correlation test	Pearson	Spearman
One group (comparison with specified theoretical distribution)	Z-test, t-test	Kolmogorov-Smirnov 1-sample test, Runs test
Independent measures, 2 groups	Independent-measures Student t-test	Kolmogorov-Smirnov 2-sample test, Mann-Whitney test
Independent measures, >2 groups	One-way, independent-measures ANOVA	Kruskal-Wallis test
Repeated measures, 2 conditions	Matched-pair t-test	Wilcoxon test
Repeated measures, >2 conditions	One-way, repeated measures ANOVA	Friedman's test

Parametric vs non-parametric techniques

Parametric technique: forward-fitting (FF) method

The LF form is predefined ➡ The LF is convolved with the observational biases ➡
➡ Fitting this function to the observed L_{iso} distribution ➡ LF parameters

Non-parametric statistical techniques are applicable to cosmological evolutions of **quasars** (Maloney & Petrosian 1999; Singal et al. 2011, 2013),
GRBs (Lloyd-Ronning et al. 2002; Kocevski & Liang 2006; Dainotti et al. 2013),
and **AGNs (blazars)** (Singal et al. 2012, Singal et al. 2014).

Joint Russian-US Konus-*Wind* experiment

- Two detectors (S1 and S2) are located on opposite faces of spacecraft, observing correspondingly the southern and northern celestial hemispheres;
- ~100-160 cm^2 effective area;
- Now around L1 at ~7 light seconds from Earth;
- Light curves (LC): ~20 – 1500 keV ;
- Waiting mode: LS res. is 2.944 s;
- Triggered mode: LC res. is 2 ms –256 ms, from T_0-0.512 s to T_0+230 s
  128-ch spectra (20 keV – 20 MeV).

Advantages

- Wide energy band: ~20 keV–20 MeV;
- Exceptionally stable background;
- The orbit of s/c excepts interferences from radiation belts and the Earth shadowing;
- Continuous observations of all sky;
- Duty circle 95%;
- Observes almost all bright events (>10^{-6}erg cm^{-2} s^{-1}).

The burst sample

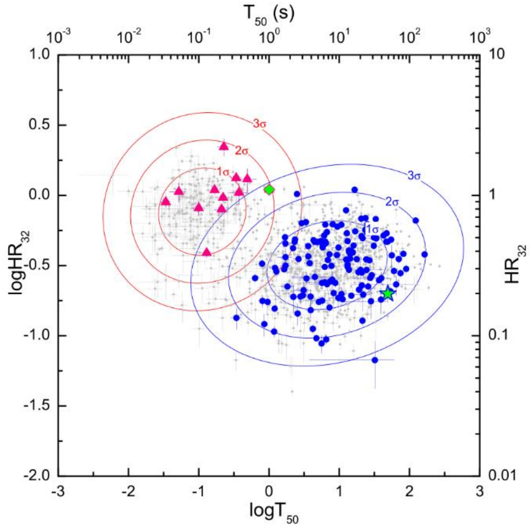

Svinkin et al. (2016)

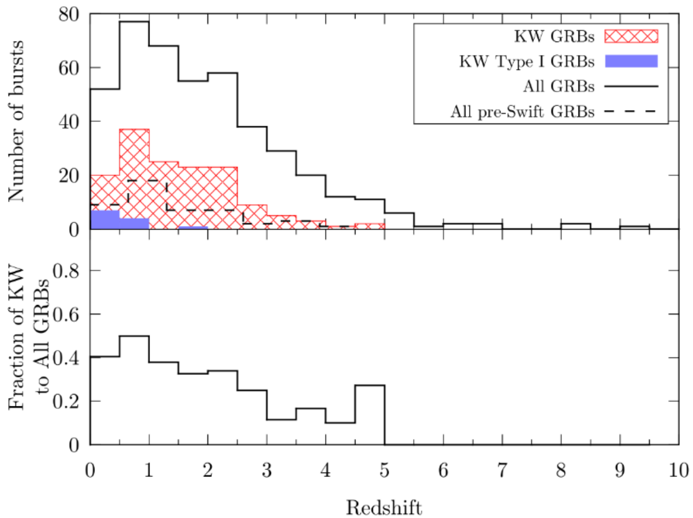

Parameter Name	Min Value	Max Value	Mean Value	Median Value
Redshift	0.096	5	1.50	1.32

- 150 GRBs (1997 Feb to 2016 Jun)
- 12 Type I (the merger-origin, typically short/hard) GRBs
- **138 Type II (the collapsar-origin, typically long/soft) GRBs**
- 32 GRBs have reasonably-constrained (from optical/IR afterglow or in two spectral band simultaneously) jet breaks times

Analysis

- The observer-frame energetics range: 10 keV – 10 MeV;
- Durations (T_{100}, T_{90}, T_{50}) were calculated in 75 keV – 1 MeV range;
- The spectral lags were estimated;
- Spectral analysis: time-integrated and peak spectra, CPL and Band models;
- Best fit model: $\chi^2_{CPL}-\chi^2_{Band}>6$ => the Band function;
- Based on the GRB redshifts, which span the range $0.1 \le z \le 5$, the rest-frame, isotropic-equivalent energies (E_{iso}) and peak luminosities (L_{iso}) were estimated;
- L_{iso} were calculated on the (1+z)64 ms time scale, which partially removes the observational bias;
- For 32 GRBs with reasonably-constrained jet breaks the collimation-corrected values of the energetics are provided.

Selection effects

Dependence of the limiting KW energy flux on E_p

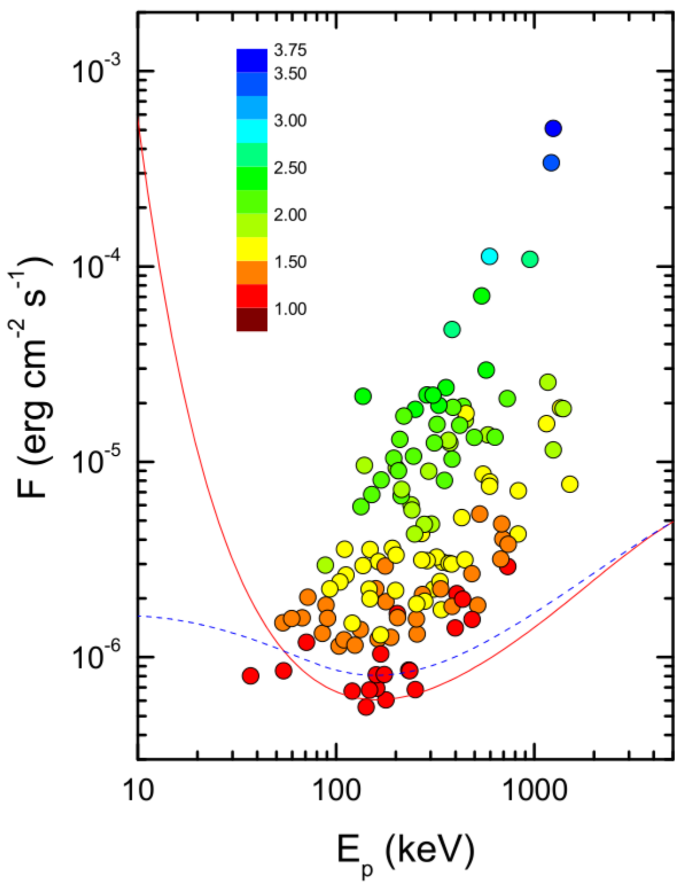

Trigger threshold: 9σ

Solid line: CPL (α= -1)

Dashed line: Band (α= -1, β = -2.5)

Incident angles: 60°

Band (2003)

Selection effects

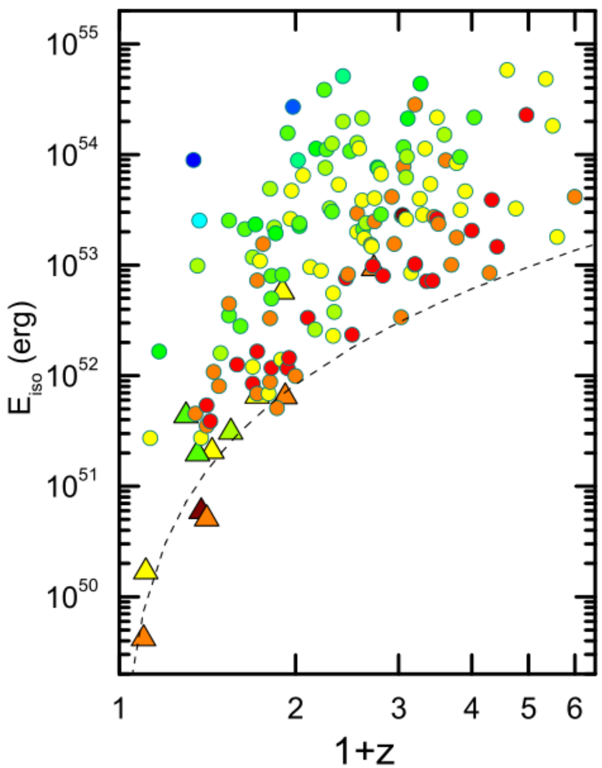

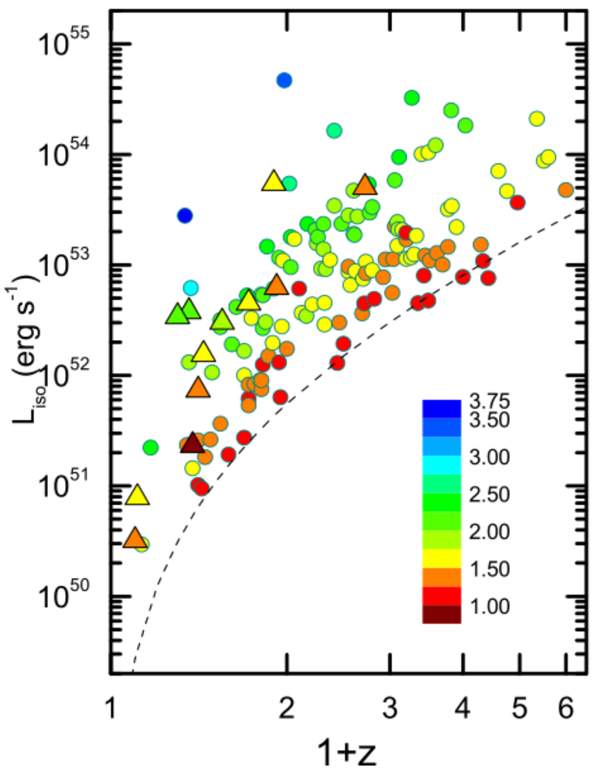

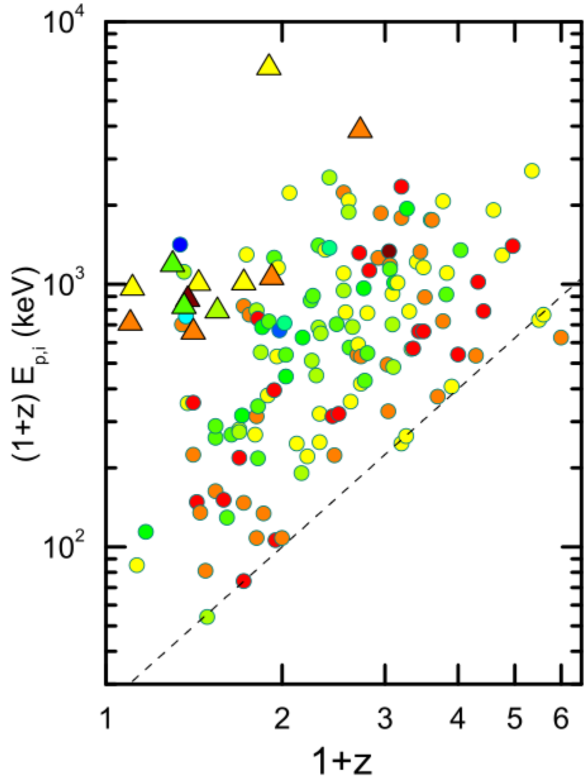

$S_{lim} \sim 3\times10^{-6}$ erg cm^{-2} $F_{lim} \sim 1\times10^{-6}$ erg cm^{-2} s^{-1} $E_{p,p,z} \sim 25(1+z)^2$ keV

GRB detection horizon

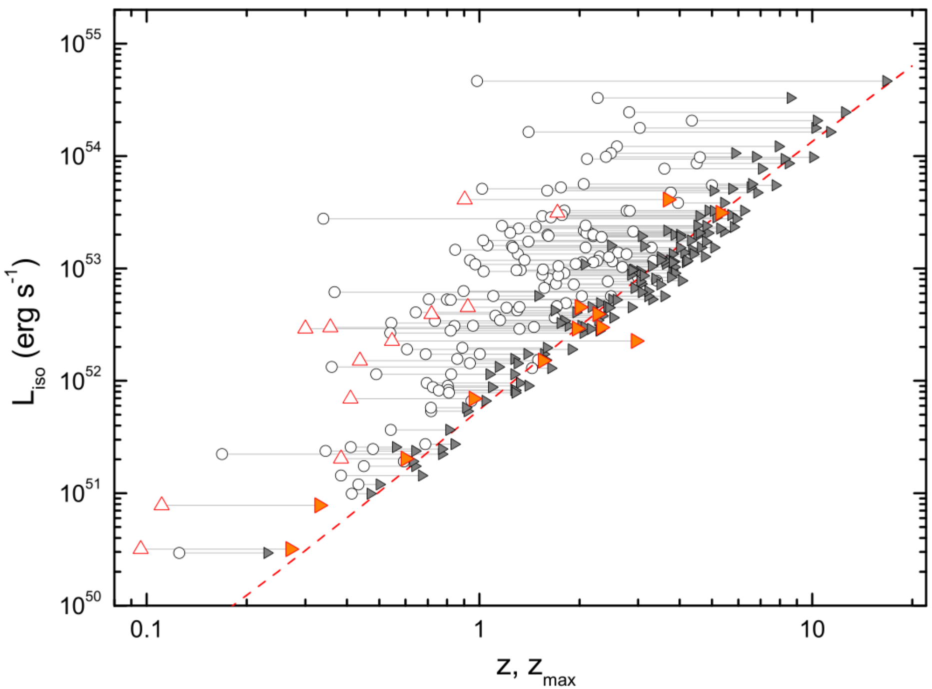

$F_{lim} = 1\times10^{-6}$ erg cm^{-2} s^{-1}

The highest z_{max}:

<u>Type I</u>

z_{max} ~ 5.3 for GRB 160410A (z_0 = 1.72)

<u>Type II</u>

z_{max} ~ 16.6 for GRB 110918A (z_0 = 0.981)

G2: ~80 – 300 keV

$$\mathrm{PCR}_z(\Delta T_{\mathrm{trig}}) = a \times \mathrm{PCR}_{z0}(a \cdot \Delta T_{\mathrm{trig}}) \times \frac{N_{\mathrm{G2}}(\alpha, \beta, a \cdot E_{\mathrm{p,p}})}{N_{\mathrm{G2}}(\alpha, \beta, E_{\mathrm{p,p}})} \times \left(\frac{D_{\mathrm{M}}(z_0)}{D_{\mathrm{M}}(z)}\right)^2$$

Trigger threshold: 9σ
Trigger time scales ΔT_{trig}: 140 ms or 1 s,
a = $(1+z_0)/(1+z)$,
$PCR_{z0}(a\Delta T_{trig})$ is reached in the observed G2 light curve on the modified time scale
$N_{G2}(\alpha,\beta,E_{pp})$ is the best spectral model count flux in G2 calculated using the DRM,
$N_{G2}(\alpha,\beta,aE_{pp})$ is the corresponding flux in the redshifted spectrum

Non-parametric statistical techniques for a truncated data sample

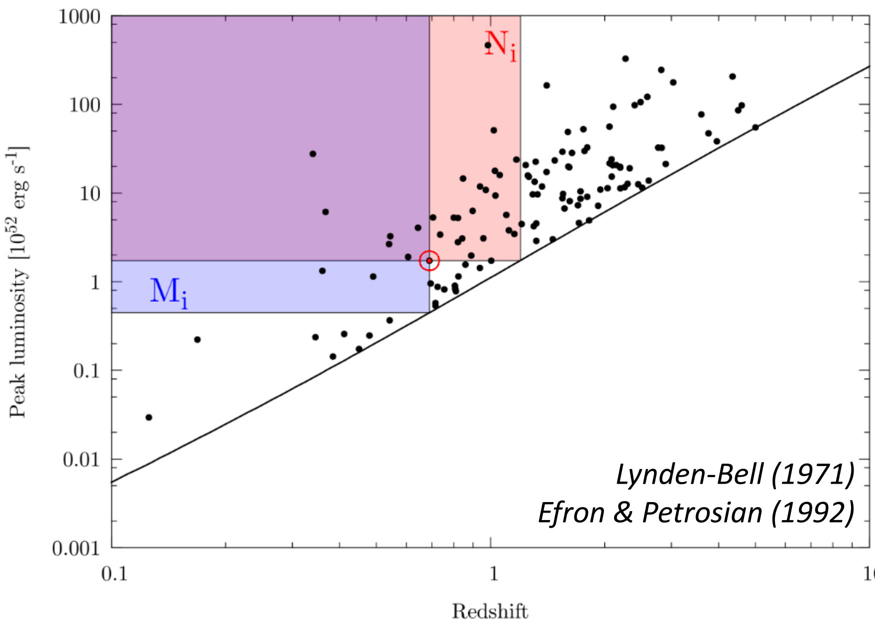

$$\ln \psi(L_i') = \sum_{j=2}^{i} \ln\left(1 + \frac{1}{N_j'}\right)$$

$$\ln \psi(z_i) = \sum_{j=2}^{i} \ln\left(1 + \frac{1}{M_j}\right)$$

Associated sets:

M

M_i: $J_i' = \{j | z_j < z_i, L_j > L_{\mathrm{lim,i}}, L_{\mathrm{i}} > L_{\mathrm{lim,j}}\}$

$$L_j > L_i^{\mathrm{lim}} \Leftrightarrow z_j^{\mathrm{lim}} > z_i$$

N_i: $J_i = \{j | L_j > L_i, L_i > L_{\mathrm{lim,j}}\}$

$$\Updownarrow$$

$$J_i = \{j | L_j > L_i, z_j < z_{\mathrm{lim,i}}\}$$

Luminosity (energy release) evolution

$$\tau = \frac{\sum_i (R_i - E_i)}{\sqrt{\sum_i V_i}}$$

$$E_i = (N_i + 1)/2$$

$$V_i = (N_i^2 - 1)/12$$

Luminosity evolution

$$g(z) = (1+z)^\delta$$

Local (non-evolving) luminosity

$$L' = L/g(z)$$

Local LF (in the commoving frame)

$$\psi(L')(1+z)^{\delta_L}$$

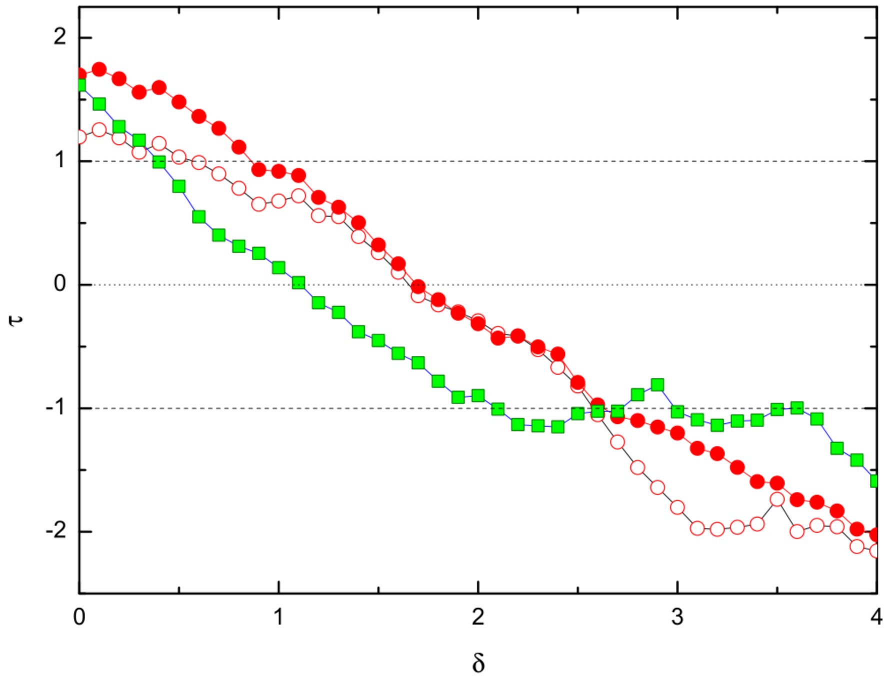

Red filled circles : per-burst truncation flux F_{lim};
red open circles: monolithic $F_{lim} = 2\times10^{-6}$ erg cm^{-2} s^{-1} ;
green squares: $S_{lim} = 4.3 \times 10^{-6}$ erg cm^{-2} .

L_{iso}: $\tau_0 = 1.7$ $\quad \delta_L = 1.7^{+0.9}_{-0.9}$ $(1\sigma$ CL)

E_{iso}: $\tau_0 = 1.6$ $\quad \delta_E = 1.1^{+1.5}_{-0.7}$

⇨ GRBs were brighter in the past

Luminosity (energy release) evolution

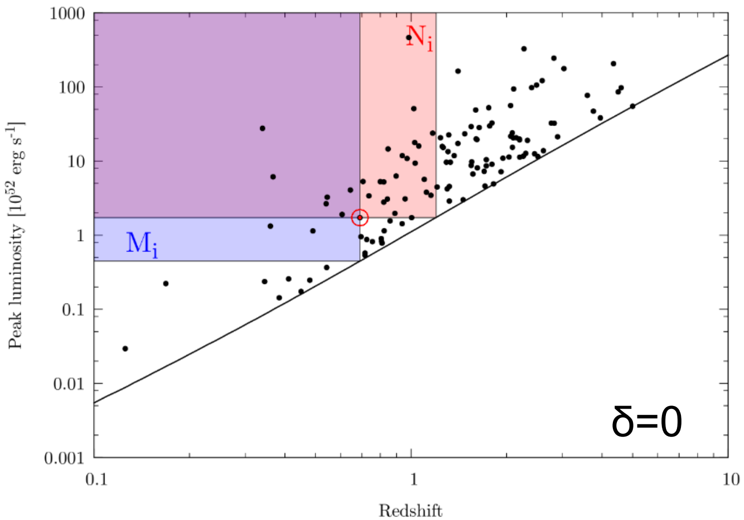

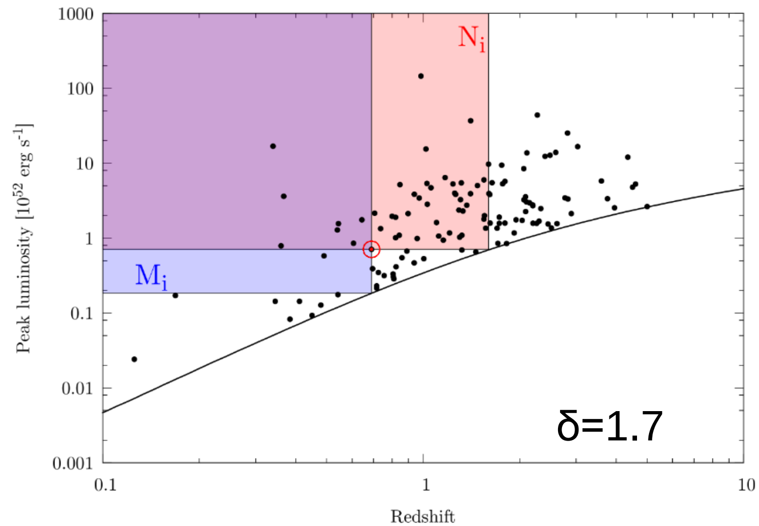

Examples of evolving astrophysical objects:

- Galaxies: the local luminosity function varies for early- and late-type galaxies (Marzke et al. 1994)
- Quasars: $L \sim (1+z)^3$, $z<1.5$ (Boyle 1993; Hewett, Foltz, & Chaffee 1993); $L \sim (1+z)^{1.5}$, $z<3$ (Hewett et al. 1993)

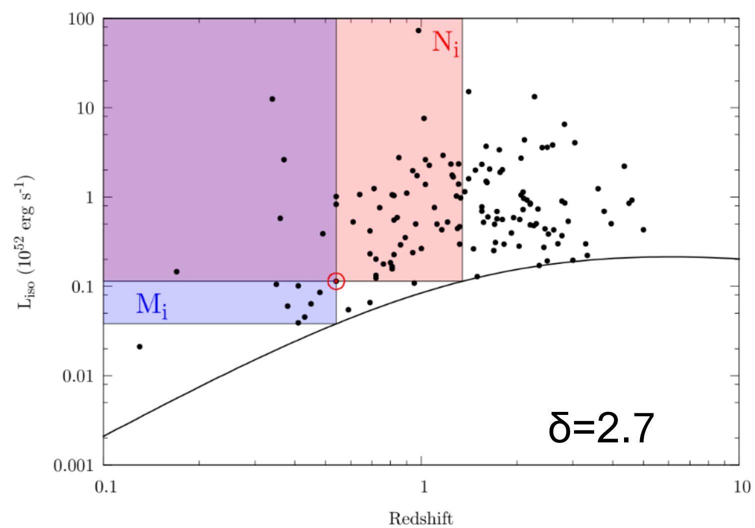

Lynden-Bell (1971)
Efron & Petrosian (1992)

Selection effects and luminosity (energy release) evolution

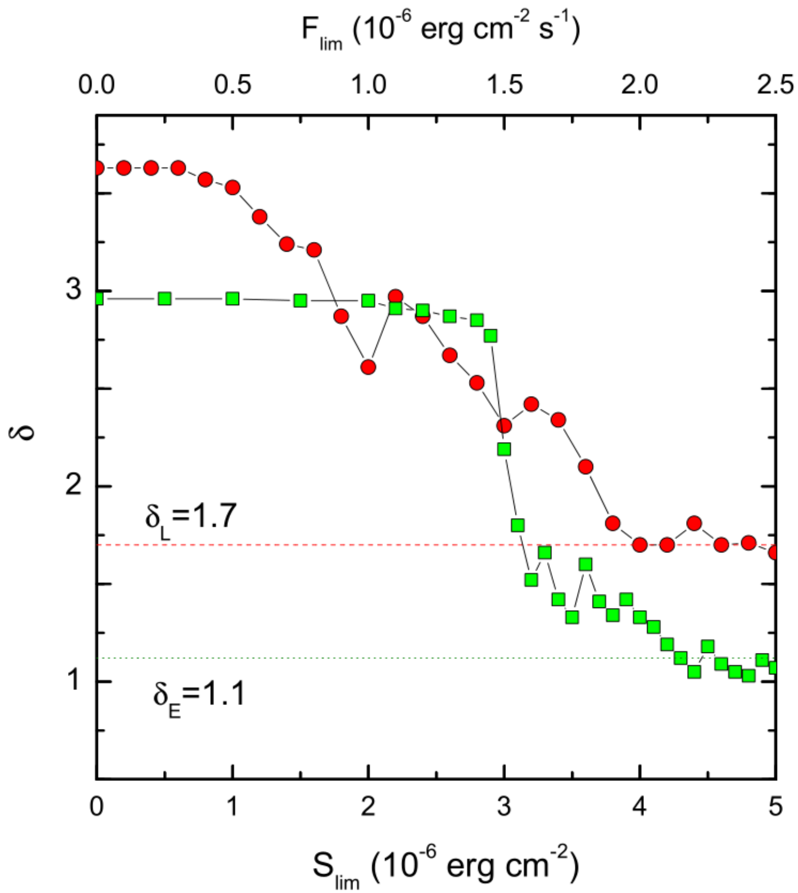

Red circles: Luminosity;
Green squares: Energy release.

$F_{lim} = 2\times10^{-6}$ erg cm^{-2} s^{-1} ;
$S_{lim} = 4.3 \times 10^{-6}$ erg cm^{-2} .

Luminosity (energy release) evolution

The evolution of the amount of energy (per unit time) emitted by the GRB progenitor (Lloyd-Ronning 2002)

The jet opening angle evolution (the jet evolution) is rejected:

$$\rho_S = -0.26$$
$$P_{\rho_S} = 0.17$$

The evolution of the GRB progenitor (massive star) itself: The stellar initial mass function (IMF) was ''top-heavy'' at high redshift (Larson 1998 and references therein, Malhotra & Rhoads 2002)

Progenitors losed less mass before collapse

The stellar metallicities were lower

The mass scale of the IMF was higher in the earlier stages of the Universe

Temperature in star-forming clouds in the early universe was probably higher

- The cosmic background temperature was higher;
- The metallicity was lower, which implies lower cooling rates and therefore higher temperatures on average;
- The heating rates were probably higher in the past because the SFR per unit volume was higher, leading to more intense radiation fields at high redshifts.

The present-time GRB luminosity and energy release functions

Cumulative luminosity function: $\ln \psi(L'_i) = \sum_{j=2}^{i} \ln \left(1 + \frac{1}{N'_j}\right)$

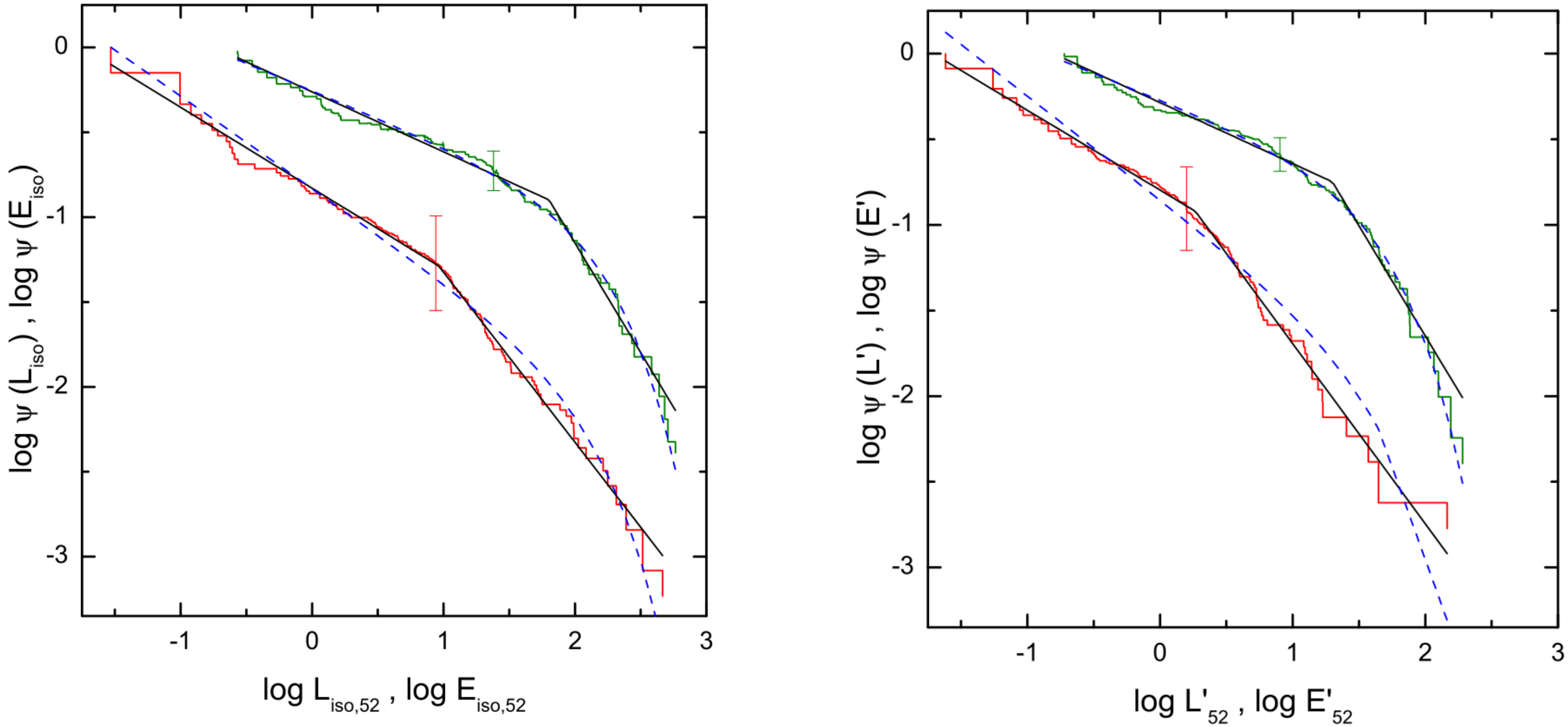

Left panel: LF (red stepped graph) and EF (green stepped graph) estimated under the assumption of no evolution of L_{iso} and E_{iso} with z; the solid and dashed lines show the best BPL and CPL fits, respectively. Right panel: present-time LF and EF estimated accounting for the luminosity and energy evolutions.

The present-time GRB luminosity and energy release functions

BPL:

$$\psi(x) \propto \begin{cases} x^{\alpha_1}, & x \le x_b \\ x_b^{(\alpha_1-\alpha_2)} x^{\alpha_2}, & x > x_b \end{cases}$$

α_1, α_2 – PL indices at the dim and bright distribution segments,
x_b – breakpoint of the distribution.

CPL:

$$\psi(x) \propto x^{\alpha} \exp(-x/x_{\rm cut})$$

α – PL index,
x_{cut} – cutoff luminosity (or energy).

Data	Evolution (PL index)	Model	χ^2(d.o.f.)	α_1	α_2	$\log x_b$ ($\log x_{\rm cut}$)
$\psi(L')$	δ_L=1.7	BPL	2.05 (133)	-0.47 ± 0.06	-1.05 ± 0.11	0.27 ± 0.12
$\psi(L')$	δ_L=1.7	CPL	18.5 (134)	-0.60 ± 0.04		2.10 ± 0.15
$\psi(E')$	δ_E=1.1	BPL	19.2 (126)	-0.36 ± 0.01	-1.28 ± 0.11	1.30 ± 0.04
$\psi(E')$	δ_E=1.1	CPL	12.7 (127)	-0.31 ± 0.02		2.09 ± 0.04
$\psi(L_{\rm iso})$	no evolution	BPL	2.32 (133)	-0.47 ± 0.06	-1.00 ± 0.10	0.96 ± 0.15
$\psi(L_{\rm iso})$	no evolution	CPL	8.90 (134)	-0.54 ± 0.04		2.58 ± 0.11
$\psi(E_{\rm iso})$	no evolution	BPL	17.2 (126)	-0.35 ± 0.01	-1.29 ± 0.12	1.80 ± 0.05
$\psi(E_{\rm iso})$	no evolution	CPL	15.4 (127)	-0.32 ± 0.01		2.63 ± 0.04

GRB formation rate evolution

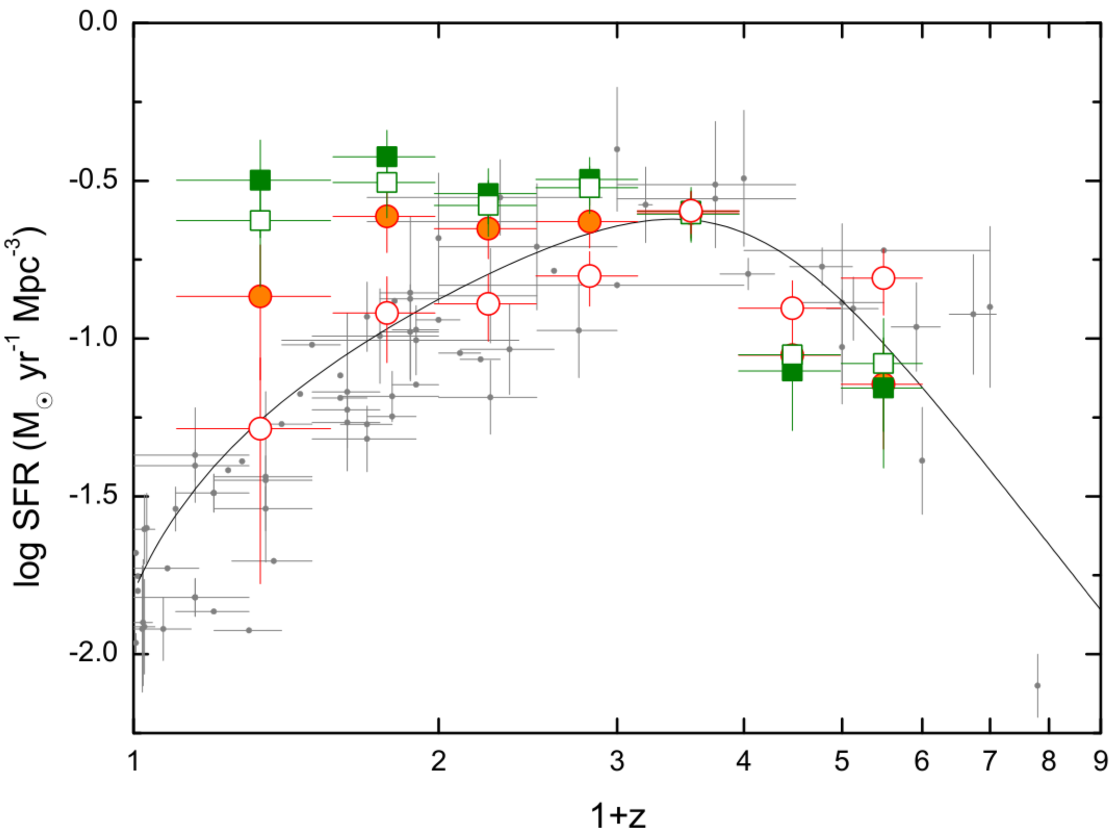

Cumulative rate evolution:

$$\ln \psi(z_i) = \sum_{j=2}^{i} \ln \left(1 + \frac{1}{M_j}\right)$$

Comoving density rate:

$$\rho(z) = \frac{d\psi}{dz}(1+z)\left(\frac{dV(z)}{dz}\right)^{-1}$$

Differential comoving volume:

$$\frac{dV(z)}{dz} = \frac{4\pi D_{\mathrm{H}} D_{\mathrm{M}}^2}{E(z)}$$

D_M is the transverse comoving distance

Hubble distance: $D_{\mathrm{H}} = c/H_0$

Normalized Hubble parameter:

$$E(z) = \sqrt{\Omega_{\mathrm{M}}(1+z)^3 + \Omega_\Lambda}$$

SFR: Hopkins (2004), Bouwens et al. (2011), Hanish et al. (2006), Thompson et al. (2006), Li (2008).

Red open circles: no luminosity evolution; red filled circles: δ_L= 1.7;
green open squares: no energy evolution; green filled squares: δ_L = 1.1.

Summary

- A systematic study of 150 GRBs (from 1997 February to 2016 June) with known redshifts was performed;
- The influence of instrumental selection effects on the GRB parameter distributions was analyzed: the regions above the limits, corresponding to the bolometric fluence

$S_{lim} \sim 3\times10^{-6}$ erg cm^{-2} (in the $E_{iso} - z$ plane) and bolometric peak energy flux

$F_{lim} \sim 1\times10^{-6}$ erg cm^{-2} s^{-1} (in the $L_{iso} - z$ plane) may be considered free from the selection biases;

- KW GRB detection horizon extends to $z_{max} \sim 16.6$, stressing the importance of GRBs as probes of the early Universe;
- The GRB luminosity evolution, luminosity and energy release functions, and the evolution of the GRB formation rate were estimated accounting for the instrumental bias:
  - The derived luminosity evolution and isotropic energy evolution indices $\delta_L \sim 1.7$ and $\delta_E \sim 1.1$ are more shallow than those reported in previous studies, albeit within errors;
  - The shape of the derived LF is best described by the broken PL function with low- and high-luminosity slopes ~ -0.5 and ~ -1, respectively;
  - The EF is better described by the exponentially-cutoff PL with the PL index ~ -0.3 and a cutoff isotropic energy of $\sim (2 - 4) \times 10^{54}$ erg;
  - **The derived GRBFR features an excess over the SFR at $z < 1$;**
- **GRBs were more luminous in the past than today.**

Thank you!